Inorganic Chemistry

pubs.acs.org/IC

Article

Solvent Templating and Structural Dynamics of Fluorinated 2D Cu-Carboxylate MOFs Derived from the Diffusion-Controlled Process

Michał K. Leszczyński, Iwona Justyniak, Krzysztof Gontarczyk, and Janusz Lewiński*

Cite This: *Inorg. Chem.* 2020, 59, 4389−4396

Read Online

ACCESS | Metrics & More | Article Recommendations | Supporting Information

ABSTRACT: The layered 2D MOFs, owing to their enhanced flexibility and tunability, have recently emerged as a promising alternative to the 3D microporous MOFs in the quest for novel responsive functional materials. However, maintaining the simultaneous control over self-assembly of molecular building blocks as well as ordered stacking of MOF layers poses a significant synthetic challenge. We report on the controlled 2D MOF formation based on a case study of solvent-templated growth of a series of 2D Cu(II)−carboxylate MOFs varying in stacking modes and distances using a diffusion-controlled MOF deposition approach in various solvent mixtures. Moreover, we demonstrate the structural dynamics of the developed 2D MOFs involving both in-plane and out-of-plane movements of the individual 2D layers triggered by solvent exchange, which allowed for selective postsynthetic transformations between the developed 2D MOFs. We also investigated the gas adsorption properties of the developed MOFs, which demonstrates a remarkable crystal size effect on the N_2 adsorption capacity using a model 2D MOF system.

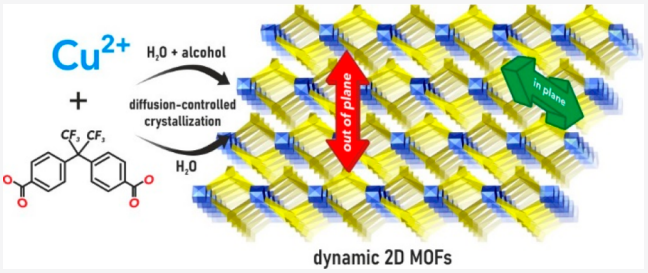

INTRODUCTION

Metal−organic frameworks (MOFs) composed of organic linkers and inorganic nodes have been attracting the immense attention of researchers due to their diverse and strikingly robust architectures combined with high surface areas and great chemical diversity. As a result, MOFs have found numerous applications in gas storage and separation, catalysis, sensors, energy storage, etc.[1−6] One of the strategies for enhancing the functionality of MOFs involves the use of fluorinated ligands, which greatly influence the material properties such as hydrophobicity, chemical stability, gas adsorption, and separation capabilities, due to specific chemical characteristics of the fluorine-containing moieties.[7−11] Moreover, rational introduction of highly electronegative fluorine atoms might allow for a fine-tuning of the electronic properties of MOFs such as luminescence or conductivity.[12] However, to fully take advantage of the structure-related properties of MOFs, their formation must be adequately controlled in order to achieve hybrid materials of desired properties.[13] One of the ongoing challenges in the rational synthesis of MOFs is related to the MOFs isomerism, i.e., the ability to adopt multiple structural arrangements of the same building blocks leading to a number of materials with different properties.[14,15] An efficient and simple solution of this issue is the use of various template molecules for the controlled MOF growth, which has already been demonstrated as a powerful approach for synthesis and formulation of desired MOFs.[16,17] In particular, the use of inherently present solvent molecules as templates for MOFs self-assembly appears as a very promising, but it is an often underdeveloped strategy. In fact, replacing one solvent for another in a typical solvothermal MOF synthesis procedure usually requires adjustment of other variables (temperature, concentrations, additives, etc.) for efficient MOF crystallization, which hinders the inference on solvent-templating in MOF synthesis.[18,19]

Over the last two decades, the continuously developed methods of MOFs synthesis and crystal engineering have led to the discovery of countless of new MOF structures.[20] This immense effort has been mostly driven by the application-oriented approach utilizing MOF rigid networks and well-defined porosity for practical aspects. However, some applications require substantial structural tunability and responsiveness of the applied porous materials, which can be achieved by rational synthetic design of the MOF networks using flexible or reactive linkers and nodes or by a postsynthetic modification strategy introducing the desired functionality to the prepared frameworks.[21−23] Within the pursuit for responsive MOFs, 2D-layered materials have emerged as a promising alternative to the 3D frameworks due to their enhanced network flexibility and ability to adopt various stacking modes and distances of 2D MOF sheets.[24,25] This structural isomerism is determined by cooperative

Received: November 27, 2019
Published: March 18, 2020

https://dx.doi.org/10.1021/acs.inorgchem.9b03472
Inorg. Chem. 2020, 59, 4389−4396

supramolecular interactions between individual layers as well as potential guest molecules, which can be controlled by the use of templates influencing the molecular and supramolecular MOFs self-assembly processes.[18,19] Interestingly, the stacking geometry of individual layers in 2D MOFs can also be adjusted dynamically by introduction or removal of various guest molecules within the premade MOF structure. As a result, the 2D layers might perform motion either in-plane ("sliding" movement, Figure 1a) or out-of-plane (Figure 1b), which leads

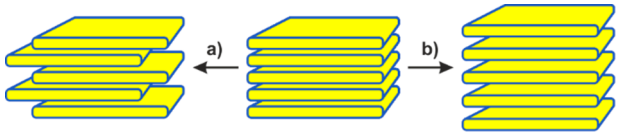

Figure 1. Two types of movement demonstrating typical structural dynamics of 2D-layered MOFs: in-plane (a) and out-of-plane (b).

to significant structural changes, e.g., opening/closing the 1D pores perpendicular to the 2D sheets[26−28] or changing the stacking distance between the individual layers.[29,30] The structural dynamics of 2D MOFs enables their promising gas adsorption properties related to the "gate opening" mechanism, which is advantageous compared to the typical gas storage in rigid 3D structures due to the high working capacity.[31,32] Moreover, 2D MOF materials are used as precursors for ultrathin MOF nanosheets, which find many applications due to their exceptionally high surface/volume atom ratios and large surface areas.[24,33−36]

One of the prevalent synthons in 2D MOFs are $M_2(\mu\text{-}O_2CR)_4$ paddlewheel units adopting square coordination geometry, which form flat or wavy MOF layers upon self-assembly with various bicarboxylates.[37] The Cu(II)-based 2D MOFs are the most extensively studied systems in that group, which is related to their relatively high stability and straightforward solvothermal synthetic approach.[37] Known structures of Cu(II)-based 2D MOFs involve vast arrays of bicarboxylate linkers, including the aforementioned fluorinated ligand systems. For example, in the presence of Cu(II) precursors and the 4,4′-(hexafluoroisopropylidene)bisbenzoate (hfipbb) linkers, 2D MOFs are formed, which could be described using the formula [Cu(hfipbb)·Solv] (where Solv = various solvent molecules coordinated to the Cu centers). The literature data includes four examples of Cu(hfipbb) structures, all prepared in solvothermal conditions, which differ in internal structure of the networks, interpenetration, as well as layer stacking distance and geometry, which results from varying preparation conditions (Figure 2).[38−41] Similar variations have also been observed for other 2D MOF systems, which indicates that their supramolecular structure can be influenced by various subtle effects like solvent type, temperature, pH, additives, etc.[14,15]

Stemming from our interest in development of efficient preparation of hybrid inorganic−organic materials,[30,43−48] herein we report on the solvent templating effect on the self-assembly of $Cu_2(\mu\text{-}O_2CR)_4$ paddlewheel units and 4,4′-(hexafluoroisopropylidene)bisbenzoate (hfipbb) linkers yielding a family of 2D MOFs (collectively identified as a **Cu(hfipbb)** family). In contrast to the previous reports,[38−41] we applied the diffusion-controlled MOF synthesis methodology, involving the MOF formation in a very low precursor concentration regime.[30] Using various solvent mixtures, we isolated and structurally characterized five members of the

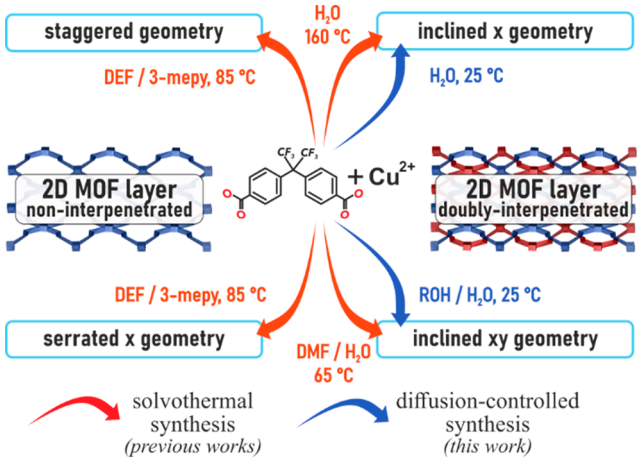

Figure 2. Overview of the 2D MOFs formed by Cu^{2+} and hfipbb linkers including data from the literature (solvothermal synthesis, red arrows) and this work (diffusion-controlled synthesis, blue arrows). Geometry of 2D layers stacking was named in accordance to the literature data.[42] 3-mepy = 3-methylpyridine.

Cu(hfipbb) family, which differ in both stacking geometry (I-*x* vs I-*xy*) and distance between the 2D layers (Figure S1). We also demonstrate the structural dynamics of the developed MOFs involving both in-plane and out-of-plane movements of the 2D layers, triggered by exchange or removal of the guest solvent molecules (Figure 3). Remarkably, the revealed transitions between various members of the **Cu(hfipbb)** family are selectively allowed or disallowed based on the type of the substrate and guest molecules.

EXPERIMENTAL SECTION

Materials and Methods. All chemicals were purchased from commercial sources and used without further purification. Potassium 4,4′-(hexa-fluoroisopropylidene)bisbenzoate solution was prepared by mixing appropriate amounts of KOH and 4,4′-(hexa-fluoroisopropylidene)bisbenzoic acid in water until all of the solids were dissolved and the pH of the solution was close to neutral. PXRD data were collected on the Empyrean diffractometer (PANalytical) employed with Ni-filtered Cu Kα radiation (40 kV, 40 mA) using Bragg−Brentano geometry and a Si zero-background holder. VTPXRD data were collected using the above instrument equipped with the Anton Paar TTK-450 sample chamber, which was evacuated (10^{-2} mbar) during the measurements. IR spectra were recorded using the FTIR Bruker-Tensor II system. Gas sorption studies were undertaken using a Micromeritics Instrument Corporation (Norcross, Georgia, USA) ASAP 2020 system. Approximately 100−150 mg of the corresponding solid product was transferred to a preweighed sample tube and evacuated under vacuum at 100 °C on the gas adsorption apparatus until the outgas rate was <5 μmHg. All gases used were of 99.999% purity. Helium was used for the free space determination after sorption analysis. Adsorption isotherms of N_2 and H_2 were measured at 77 K in a liquid nitrogen bath. Adsorption isotherms of CO_2 were measured at 273 and 298 K in methanol bath controlled by circulating refrigerated medium. Elemental analyses were carried out with an UNICUBE Elementar Analyzer (GmbH). SEM imaging was performed using FEI Nova NanoSEM 450 system equipped with a field emission electron gun operating at 2 kV. The optical microscope images were collected using the Olympus BX53 microscope.

Synthesis of $[Cu(hfipbb)\cdot H_2O]_{I\text{-}x}$ (1). Solutions of copper(II) nitrate trihydrate (241.6 mg, 1.0 mmol, in 2 mL of H_2O) and potassium 4,4′-(hexa-fluoroisopropylidene)bisbenzoate (1 mmol, in 2 mL of H_2O) were prepared. The solutions were placed in a special glass reactor that prevented mixing of the substrates (Figure S2). Next, the reactor was gently filled with water to create a diffusion path

https://dx.doi.org/10.1021/acs.inorgchem.9b03472
Inorg. Chem. 2020, 59, 4389−4396

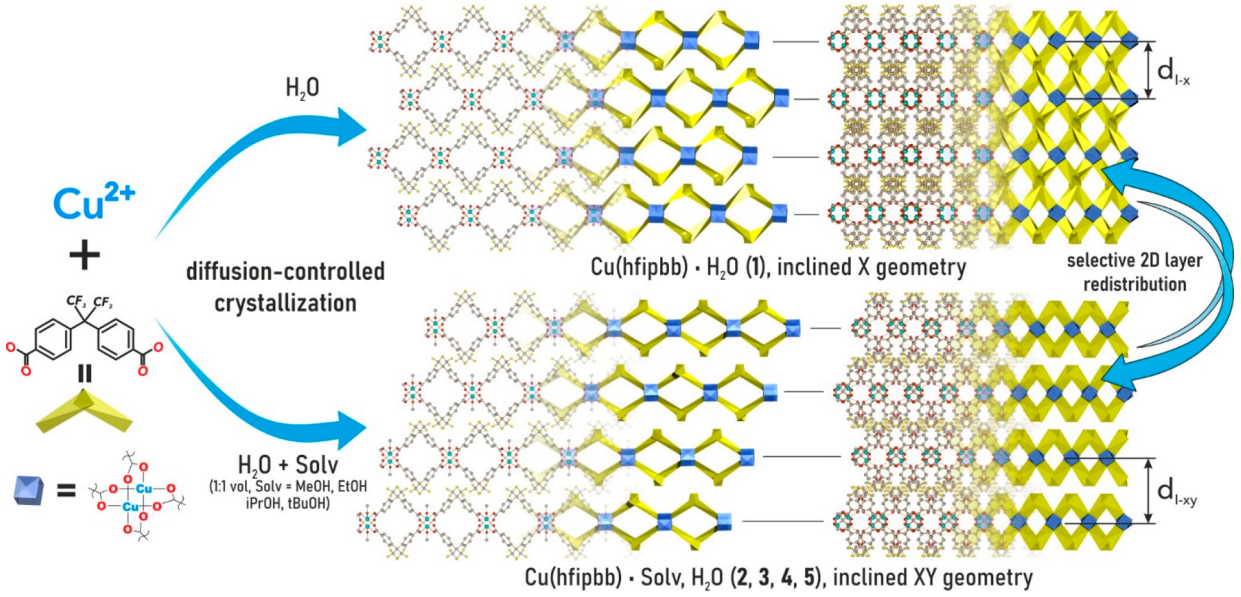

Figure 3. Schematic representation of the synthesis of various members of the **Cu(hfipbb)** family and their postsynthetic structural dynamics, $d_{I\text{-}x}$ = 11.02 Å (in **1**), $d_{I\text{-}xy}$ = 12.80 Å (in **2**), 12.78 Å (in **3**), 13.52 Å (in **4**), and 14.81 Å (in **5**). Note: interlayer stacking distances in studied 2D MOFs are dependent on temperature (values reported here for 100 K).

between substrates. The diffusion controlled process was conducted for 4 weeks at room temperature which resulted in formation of turquoise flake-shaped single crystals of **1**. The product was collected and washed with water and THF and dried in vacuo. PXRD analysis confirmed the phase purity of the product. Yield: 370 mg (78%). Elemental analysis (%) cacld for $[C_{17}H_8O_4F_6Cu{\cdot}1.15\ H_2O]$: C 43.03, H 2.19; found C 43.03, H 2.19.

Synthesis of [Cu(hfipbb)·MeOH]$_{I\text{-}xy}$ (2). Synthesis of flake-shaped single crystals of **2** was performed by the same procedure as for **1** with exception that H_2O/MeOH mixture (1:1 by volume) was used instead of H_2O. Yield: 365 mg (75%). Elemental analysis (%) cacld for $[C_{17}H_8O_4F_6Cu{\cdot}0.95\ MeOH{\cdot}0.17\ H_2O]$: C 44.24, H 2.51; found C 44.24, H 2.51. Synthesis of the microcrystalline powder of **2** was performed in the following way: solutions of copper(II) nitrate trihydrate (241.6 mg, 1.0 mmol, in 2 mL of H_2O/MeOH mixture (1:1 by volume)) and potassium 4,4′-(hexa-fluoroisopropylidene)-bisbenzoate (1 mmol, in 2 mL of H_2O/MeOH mixture (1:1 by volume)) were mixed at RT, which resulted in an immediate formation of a turquoise precipitate. The reaction mixture was centrifuged, and the liquid phase was removed. The resulting solid was washed with THF and dried in vacuo. PXRD analysis confirmed the phase purity of the product. Yield: 460 mg (95%). Elemental analysis (%) cacld for $[C_{17}H_8O_4F_6Cu{\cdot}0.87\ MeOH{\cdot}0.12\ H_2O]$: C 44.36, H 2.44; found C 44.36, H 2.44.

Synthesis of [Cu(hfipbb)·EtOH]$_{I\text{-}xy}$ (3). Synthesis of flake-shaped single crystals of **3** was performed by the same procedure as for **1** with the exception that an H_2O/EtOH mixture (1:1 by volume) was used instead of H_2O. Yield: 410 mg (82%). Elemental analysis (%) cacld for $[C_{17}H_8O_4F_6Cu{\cdot}0.97\ EtOH{\cdot}0.11\ H_2O]$: C 45.46, H 2.83; found C 45.47, H 2.83.

Synthesis of [Cu(hfipbb)·*i*PrOH]$_{I\text{-}xy}$ (4). Synthesis of flake-shaped single crystals of **4** was performed by the same procedure as for **1** with the exception that an H_2O/*i*PrOH mixture (1:1 by volume) was used instead of H_2O. Yield: 438 mg (85%). Elemental analysis (%) cacld for $[C_{17}H_8O_4F_6Cu{\cdot}0.99\ iPrOH{\cdot}0.09\ H_2O]$: C 46.58, H 3.15; found C 46.58, H 3.15.

Synthesis of [[Cu(hfipbb)·H$_2$O]·*t*BuOH]$_{I\text{-}xy}$ (5). Synthesis of flake-shaped single crystals of **5** was performed by the same procedure as for **1** with the exception that an H_2O/*t*BuOH mixture (1:1 by volume) was used instead of H_2O. Yield: 427 mg (72%). Elemental analysis (%) cacld for $[C_{17}H_8O_4F_6Cu{\cdot}1.63\ tBuOH{\cdot}1.05\ H_2O]$: C 47.60, H 4.48; found C 47.60, H 4.48.

X-ray Structure Determination. The crystals of all complexes were selected under Paratone-N oil, mounted on the nylon loops, and positioned in the cold stream on the diffractometer. The X-ray data for materials **1**, **2**, **3**, **4**, and **5** were collected at 100(2) K on a SuperNova Agilent diffractometer using Mo Kα radiation (λ = 0.71073 Å).[49] The structures were solved by direct methods and refined using SHELXL-2018/3.[50] All non-hydrogen atoms were refined with anisotropic displacement parameters. Hydrogen atoms attached to carbon atoms were added to the structure model at geometrically idealized coordinates and refined as riding atoms.

Crystal Data for ***1****,* $[Cu(hfipbb){\cdot}H_2O]_{I\text{-}x}$. $C_{17}H_{10}CuF_6O_5$: M = 471.79, monoclinic, space group P 2/n (no. 13), a = 12.6099(4) Å, b = 6.9479(3) Å, c = 20.6847(7) Å, β = 93.151(3)°, U = 1809.49(11) Å^3, Z = 4, $F(000)$ = 940, D_c = 1.732 g cm^{-3}, μ(Cu−Kα) = 1.294 mm^{-1}, θ_{max} = 29.054°, 4186 unique reflections. Refinement converged at R_1 = 0.0567, wR_2 = 0.1163 for all data and 262 parameters (R_1 = 0.0461, wR_2 = 0.1117 for 3526 reflections with $I_0 > 2\sigma(I_0)$). The goodness-of-fit on F^2 was equal to 1.127. The weighting scheme $w = [\sigma^2(F_0)^2 + (0.0418P)^2 + 3.1964P]^{-1}$ where $P = (F_0^2 + 2F_c^2)/3$ was used in the final stage of refinement. The residual electron density = +0.80/−0.82 eÅ^{-3}. CCDC no. 1961201.

Crystal Data for ***2****,* $[Cu(hfipbb){\cdot}MeOH]_{I\text{-}xy}$. $C_{18}H_{12}CuF_6O_5$: M = 485.73, monoclinic, space group C 2/c (no. 15), a = 28.048(2) Å, b = 6.9826(2) Å, c = 22.8971(12) Å, β = 114.083(5)°, U = 4094.0(4) Å^3, Z = 8, $F(000)$ = 1944, D_c = 1.576 g cm^{-3}, μ(Cu−Kα) = 1.146 mm^{-1}, θ_{max} = 28.881°, 6964 unique reflections. Refinement converged at R_1 = 0.0867, wR_2 = 0.2089 for all data and 276 parameters (R_1 = 0.0727, wR_2 = 0.1932 for 5680 reflections with $I_0 > 2\sigma(I_0)$). The goodness-of-fit on F^2 was equal to 1.071. The weighting scheme $w = [\sigma^2(F_0)^2 + (0.0418P)^2 + 3.1964P]^{-1}$ where $P = (F_0^2 + 2F_c^2)/3$ was used in the final stage of refinement. The residual electron density = +3.82/−1.32 eÅ^{-3}. CCDC no. 1961202.

Crystal Data for ***3****,* $[Cu(hfipbb){\cdot}EtOH]_{I\text{-}xy}$. $C_{19}H_{14}CuF_6O_5$: M = 499.84, monoclinic, space group I 2/a (no. 15), a = 23.594(5) Å, b = 6.989(5) Å, c = 27.120(5) Å, β = 109.514(5)°, U = 4215(3) Å^3, Z = 8, $F(000)$ = 2008, D_c = 1.575 g cm^{-3}, μ(Cu−Kα) = 1.116 mm^{-1}, θ_{max} = 29.172°, 4193 unique reflections. Refinement converged at R_1 = 0.1243, wR_2 = 0.2471 for all data and 280 parameters (R_1 = 0.0873, wR_2 = 0.2264 for 2864 reflections with $I_0 > 2\sigma(I_0)$). The goodness-of-fit on F^2 was equal to 0.987. The weighting scheme $w = [\sigma^2(F_0)^2 + (0.0418P)^2 + 3.1964P]^{-1}$ where $P = (F_0^2 + 2F_c^2)/3$ was used in the

https://dx.doi.org/10.1021/acs.inorgchem.9b03472
Inorg. Chem. 2020, 59, 4389−4396

final stage of refinement. The residual electron density = +1.79/−1.69 eÅ^{-3}. CCDC no. 1961203.

Crystal Data for **4**, *[Cu(hfipbb)·iPrOH]$_{I\text{-}xy}$*. $C_{20}H_{16}CuF_6O_5$: M = 513.87, monoclinic, space group I 2/a (no. 15), a = 23.5090(11) Å, b = 7.0185(3) Å, c = 28.0864(10) Å, β = 105.679(4)°, U = 4461.8(3) Å^3, Z = 8, $F(000)$ = 2072, D_c = 1.530 g cm^{-3}, μ(Cu−Kα) = 1.056 mm^{-1}, θ_{max} = 26.497°, 4597 unique reflections. Refinement converged at R_1 = 0.0818, wR_2 = 0.1988 for all data and 308 parameters (R_1 = 0.0718, wR_2 = 0.1908 for 3915 reflections with $I_0 > 2\sigma(I_0)$). The goodness-of-fit on F^2 was equal to 1.075. The weighting scheme $w = [\sigma^2(F_0)^2 + (0.0418P)^2 + 3.1964P]^{-1}$ where $P = (F_0^2 + 2F_c^2)/3$ was used in the final stage of refinement. The residual electron density = +2.80/−0.56 eÅ^{-3}. CCDC no. 1961204.

Crystal Data for **5**, *[[Cu(hfipbb)·H$_2$O]·tBuOH]$_{I\text{-}xy}$*. $C_{46}H_{50}Cu_2F_{12}O_{13}$: M = 1165.94, monoclinic, space group I 2/a (no. 15), a = 30.2182(16) Å, b = 6.9999(4) Å, c = 23.1075(9) Å, β = 101.508(4)°, U = 4789.5(4) Å^3, Z = 4, $F(000)$ = 2384, D_c = 1.617 g cm^{-3}, μ(Cu−Kα) = 0.999 mm^{-1}, θ_{max} = 26.499°, 6736 unique reflections. Refinement converged at R_1 = 0.1098, wR_2 = 0.2444 for all data and 355 parameters, 46 restraints (R_1 = 0.0863, wR_2 = 0.2220 for 5148 reflections with $I_0 > 2\sigma(I_0)$). The goodness-of-fit on F^2 was equal to 1.033. The weighting scheme $w = [\sigma^2(F_0)^2 + (0.0418P)^2 + 3.1964P]^{-1}$ where $P = (F_0^2 + 2F_c^2)/3$ was used in the final stage of refinement. The residual electron density = +1.97/−1.10 eÅ^{-3}. CCDC no. 1961205.

RESULTS AND DISCUSSION

Synthesis and Structures of the Cu 2D MOFs. The supramolecular architectures of 2D MOFs can be affected by various subtle effects as mentioned above. In this regard, we wondered how the diffusion-controlled MOF synthesis methodology will direct the crystal structures of 2D MOFs. To this aim we selected 2D Cu-MOFs based on a paddlewheel $Cu_2(OOR)_4$ cluster and a fluorinated bicarboxylate linker as a model system. In control experiments, we used $Cu(NO_3)_2$ and K_2hfipbb salts as precursors in the diffusion-controlled synthesis in water and various water/alcohol (MeOH, EtOH, *i*PrOH, and *t*BuOH) mixtures. The reaction conducted in water yielded [Cu(hfipbb)·H$_2$O]$_{I\text{-}x}$ (**1**; the lower index indicates the 2D layers stacking type[42]) (Figure 3), which has been previously reported as the result of solvothermal synthesis in water at 160 °C.[38] However, reactions involving water/alcohol mixtures resulted in the formation of four new 2D MOF materials: [Cu(hfipbb)·MeOH]$_{I\text{-}xy}$ (**2**; prepared in H$_2$O/MeOH), [Cu(hfipbb)·EtOH]$_{I\text{-}xy}$ (**3**; H$_2$O/EtOH), [Cu(hfipbb)·*i*PrOH]$_{I\text{-}xy}$ (**4**; H$_2$O/*i*PrOH), and [[Cu(hfipbb)·H$_2$O]·*t*BuOH]$_{I\text{-}xy}$ (**5**; H$_2$O/*t*BuOH) (Figure 3), all isolated in a form of turquoise flake-shaped single crystals. The resulting materials were characterized by elemental analysis, PXRD and single-crystal X-ray diffraction (SCXRD), FTIR spectroscopy (for details see Figures S3−S7), and a gas adsorption study involving N_2, H_2, and CO_2 as adsorbates.

SCXRD analysis of the developed 2D MOFs revealed a common distinctive structural feature, namely, the presence of topologically equivalent 2D MOF layers based on $[Cu_2(OOR)_4]$ paddlewheel-type nodes connected by V-shaped hfipbb linkers. All of the observed 2D layers were composed of two independent interpenetrated networks and included 1D open channels parallel to the layer surface (Figure 4). However, the materials prepared using various solvents significantly differed in the supramolecular arrangement of the 2D layers exhibiting two stacking types (I-*x* and I-*xy*) as well as various stacking distances, which indicates a strong solvent templating effect on the supramolecular structure of the studied materials. Remarkably, these various stacking

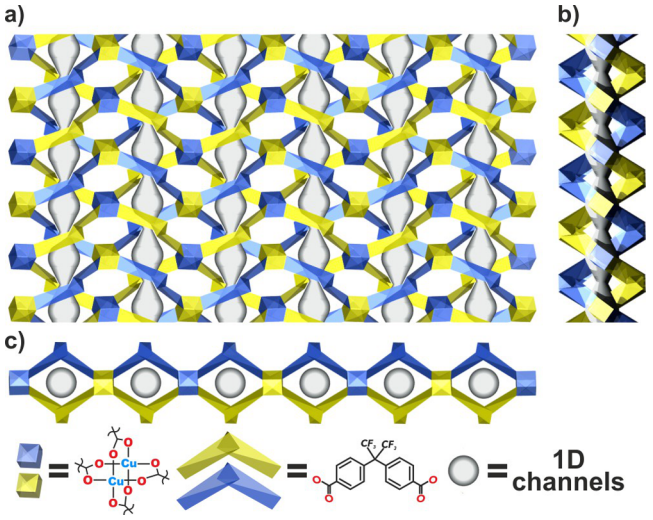

Figure 4. Common structural motif for **1**−**5**: a single layer of MOF demonstrating its doubly interpenetrated structure (independent networks displayed in blue-yellow and yellow-blue) and internal channels (displayed in gray) presented in perpendicular (a) and parallel (b, c) directions to the 2D layer surface.

arrangements were not related to the presence of any covalent or hydrogen bonding between the individual MOF sheets but rather to the weak interactions influenced by the presence of various solvent guest molecules either in the 1D channels or coordinated to the axial positions of the $[Cu_2(OOR)_4]$ paddlewheels. Notably, PXRD analysis of the studied 2D MOFs (**1**−**5**) revealed strong preferred orientation of crystals along the direction of 2D layers (Figure S8). This observation clearly indicates that the flake shape of the crystals is a result of significantly faster crystal growth in that direction. Albeit this is not unexpected for 2D-structured materials, in the case of the **Cu(hfipbb)** family, it might kinetically limit processes involving transportation of molecules through the 1D channels, which are parallel to the MOF layers (Figure 4).

As evidenced by the SCXRD study, the crystal structure of **1** is composed of $[Cu_2(OOR)_4]\cdot 2H_2O$ clusters connected by dianionic hfipbb linkers (Figure S1a), which form a 2D MOF with the interlayer distance of 11.02 Å. The axial positions of the $[Cu_2(OOR)_4]$ clusters are occupied by water molecules (Figure 5a), which can be removed by heating the material in

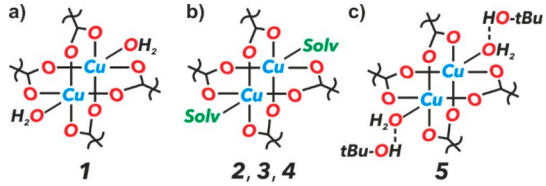

Figure 5. Cu-carboxylate clusters in the developed materials: (a) **1**, (b) **2**, **3**, and **4**, and (c) **5**. Solv = MeOH (for **2**), EtOH (**3**), or iPrOH (**4**).

vacuum at 100 °C for 3 h, resulting in a color change to sapphire-like. Detailed investigations of structural changes upon thermal treatment of **1** were conducted using the *in situ* variable temperature X-ray powder diffraction in vacuum (VTPXRD, Figure S9), which revealed a phase transition at ca. 125 °C, similar to that previously reported for analogous Cr(II)-based material.[30] The crystal structure of **2** differs from

https://dx.doi.org/10.1021/acs.inorgchem.9b03472
Inorg. Chem. 2020, 59, 4389−4396

that observed for **1** in both stacking distance (12.80 Å) and stacking type (I-*xy*) of the MOF layers, as revealed by the SCXRD analysis (Figure S1b). This structural difference is related to the MeOH molecules coordinated to the axial positions of the $[Cu_2(OOR)_4]$ units in **2** (Figure 5b), which influences the supramolecular arrangement of the MOF layers. Thermal treatment of **2** also led to desolvated sapphire-colored material, which was observed as a phase transition at ca. 75 °C in the VTXPRD study (Figure S10). Surprisingly, the product of **2** desolvation exhibited a strikingly similar PXRD pattern to **1**, which suggests that the phase transition involves a change in the 2D layer stacking geometry. Moreover, unlike any other 2D Cu-MOFs described here, **2** can be easily prepared by direct precipitation at room temperature by mixing of the solutions of $Cu(NO_3)_2$ and K_2hfipbb in H_2O/MeOH, yielding a fine blue powder of the desired 2D MOF material (**2-P**) containing microcrystals ca. 10 μm in size, as confirmed using PXRD analysis (Figure S11) and SEM imaging (Figure S12).

According to the SCXRD analysis, the crystal structures of **3** and **4** are essentially similar to that observed for **2** but differ in the type of molecule coordinated to the Cu centers (Figures 5b and S1c,d) as well as in the interlayer stacking distances (12.78 and 13.52 Å for **3** and **4**, respectively). The VTPXRD study revealed that **3** undergoes a slight phase transition at ca. 150 °C, which does not affect the layer stacking distance (Figure S13), whereas **4** did not exhibit any changes up to 200 °C (Figure S14). This observation suggests limited mobility of *i*PrOH molecules, as compared to smaller EtOH molecules, in the relatively narrow channels of the investigated MOF. Finally, the SCXRD study of **5** revealed that its supramolecular structure consists of I-*xy* stacked 2D layers with the interlayer stacking distance of 14.81 (Figure S1e). In contrary to the products **2**, **3**, and **4** prepared using MeOH, EtOH, and *i*PrOH, the Cu coordination sites in **5** were saturated by water molecules, while *t*BuOH molecules were only present inside pores, interacting by hydrogen bonding (Figure 5c). Remarkably, the presence of *t*BuOH molecules templated the MOF growth into formation of a I-*xy* stacked structure as opposed to the I-*x* stacking in the product formed in pure H_2O as solvent. However, as revealed by the PXRD study, **5** was unstable outside of the mother liquor and spontaneously decomposed into a more closely packed structure with interlayer distance of 13.71 Å after ca. 48 h of storage at RT. The same phase transition of **5** was observed in the VTPXRD study in vacuum already at 50 °C (Figure S15).

Structural Dynamics Study of the Developed 2D MOFs. As demonstrated above, the supramolecular arrangement of the 2D MOF layers in the **Cu(hfipbb)** family is heavily dependent on the type of ligands incorporated in the $[Cu_2(OOR)_4]$ units. Taking that into consideration, we wondered if both the stacking distance and the stacking mode of the studied 2D MOFs could be postsynthetically modified by a phase transition triggered by solvent exchange (Figure 6). Therefore, we have designed a series of experiments in which **1**, **2**, **3**, and **4** (**5** was excluded due to low stability) were soaked in various solvents (H_2O, MeOH, EtOH, or *i*PrOH) for 6 h, followed by PXRD analysis in order to find whether the studied members of the **Cu(hfipbb)** family can be interchangeably transformed into one another. Remarkably, the results demonstrated significant selectivity of the studied postsynthetic processes depending on the type of substrate and solvent used (Table 1, Figures S16–19). As seen from the results of this study, the transformation from **1** to **2**

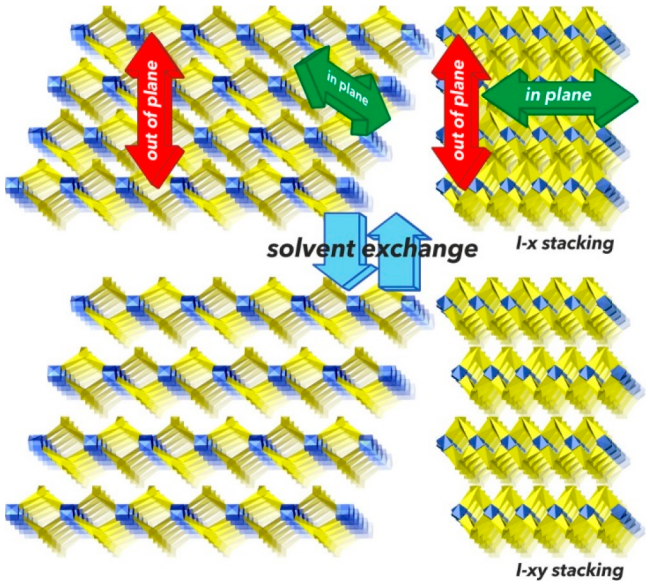

Figure 6. Schematic illustration of the solvent exchange-triggered movement of 2D layers in members of the **Cu(hfipbb)** family.

Table 1. Transformations between the Members of the Cu(hfipbb) Family

	products[a]			
substrate	+ H_2O	+ MeOH	+ EtOH	+ *i*PrOH
1	–	**2**	no reaction	no reaction
2	**1**	–	mixture[b]	no reaction
3	**1**	mixture[c]	–	no reaction
4	**1**	no reaction	no reaction	–

[a]After 6 h of soaking. [b]Mixture containing **3** and other unidentified products. [c]Mixture containing **2** and other unidentified products.

and from **2** to **1** could be easily conducted by application of the appropriate solvent (MeOH and H_2O, respectively). In a similar fashion, both **3** and **4** could be converted into **1** by soaking with H_2O, but the reverse processes from **1** to **3** and from **1** to **4** were not effective. Furthermore, both soaking **2** with EtOH and soaking **3** with MeOH yielded mixed phases. Finally, **4** proved to be unreactive toward MeOH and EtOH, and any attempts to obtain **4** by postsynthetic solvent exchange were unsuccessful. Noteworthy, as mentioned above, heating of **4** in vacuum did not lead to any structural change, while soaking **4** in water easily yielded **1**, which suggests that water molecules facilitate mobility of *i*PrOH through the narrow 1D channels in the material. The demonstrated selective transformations involving both in-plane and out-of-plane movements of MOF layers clearly indicate that the key factors influencing the network dynamics are related to the type of guest solvent molecules.

Gas Adsorption Studies. Structural analyses of the developed 2D MOFs revealed the presence of 1D channels with relatively narrow openings of 2.99, 3.12, 2.79, 2.97, and 3.16 Å (determined using the Poreblazer software)[S1] for **1**, **2**, **3**, **4**, and **5**, respectively. In order to evaluate the gas adsorption properties of the studied MOFs we initially conducted isothermal N_2 adsorption studies at 77 K involving **1**, **2**, **3**, and **4** (**5** was excluded due to low stability) after the thermal activation conducted in vacuum, which revealed low capacities of all of the investigated materials (Figure S20). This

https://dx.doi.org/10.1021/acs.inorgchem.9b03472
Inorg. Chem. 2020, 59, 4389–4396

observation is in line with kinetic diameter of N_2 (3.64 Å) being greater than the pore openings in the studied materials and indicates rigidity of the networks. To verify this explanation we decided to conduct adsorption experiments of H_2, as a smaller molecule (kinetic diameter 2.89 Å), on materials **1**, **2**, **3**, and **4**. Indeed, the observed gas adsorption capacities of H_2 (Figure S21) were significantly greater than those observed for N_2 in case of every tested material, which confirms our view. Further studies involving materials **1**−**4** revealed significant CO_2 adsorption capacities at 298 K (Figure 7) and 273 K (Figure S22). The CO_2 adsorption values of **1**, **2**, and **3** were similar and varied in the range from 20 to 27 cm^3/g at 850 mmHg; sample **4** exhibited a lower capacity of ca. 11 cm^3/g at 850 mmHg, which is in accordance with the observations mentioned above of limited ability to remove *i*PrOH molecules by thermal and vacuum treatment. The ability of the **1**−**4** to adsorb CO_2, with a kinetic diameter (3.30 Å) very similar to the pore openings, indicates that the materials are likely prone to a temperature triggered gate-opening effect.[47,52]

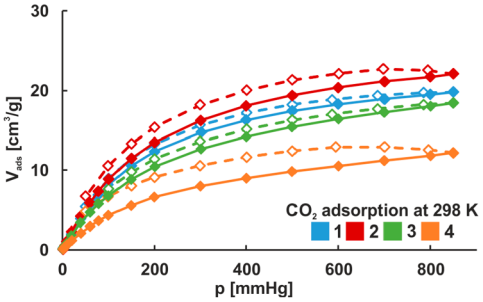

Figure 7. CO_2 adsorption isotherms at 298 K of **1** (blue), **2** (red), **3** (green), and **4** (orange). All of the samples were in a form of flake-shaped crystals. Open symbols denote desorption.

The above absorption studies were conducted using samples in the form of flake-shaped crystals; thus, we wondered if the material formulation could affect the gas adsorption capabilities of the studied materials. To this aim, we selected material **2**, which conveniently could be obtained both in the form of highly anisotropic single crystals (**2**, prepared by diffusion-controlled deposition) and fine microcrystalline powder (**2-P**, prepared by direct precipitation, crystal size ca. 10 μm, Figures S12 and S23). Remarkably, the H_2 adsorption properties of **2-P** and **2** at 77 K were dramatically different (Figure 8a), which clearly indicates that crystals of a smaller size could easily be penetrated by gas molecules. This observation of material formulation affecting its gas adsorption capabilities is likely due to the kinetic effects related to a limited number of pore entrances in the bigger flake-like crystals as well as limited mobility of the gas molecules in the narrow 1D channels. This limiting effect was observed to be alleviated at 273 and 298 K as **2** and **2-P** revealed very similar CO_2 adsorption capacities at these temperatures (Figure 8b), which suggests increased mobility through the 1D channels, probably related to the framework flexibility at higher temperatures. In order to further test the hypothesis of absorption capabilities of **2** being related to the crystal size we investigated H_2 adsorption properties of a ground sample of **2** (marked as **2-G**). To this aim, single crystals of **2** were manually ground for 10 min in an agate mortar, soaked in MeOH for 24 h, and dried, resulting in a fine powder of **2-G**.

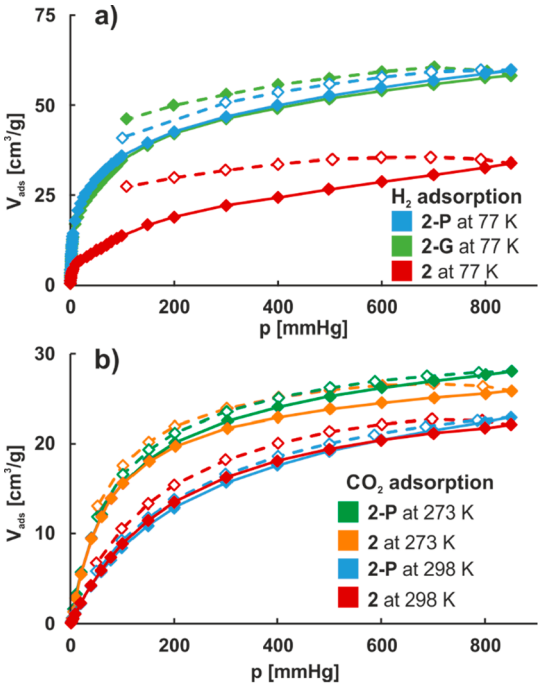

Figure 8. (a) H_2 adsorption isotherms at 77 K of **2-P** (blue), **2-G** (green), and **2** (red). (b) CO_2 adsorption isotherms at 298 K of **2-P** (blue) and **2** (red) and at 273 K of **2-P** (green) and **2** (orange). Open symbols denote desorption.

The PXRD pattern of **2-G** perfectly matched that of **2-P** (Figure S11), while the estimated crystal sizes were 50−500 μm for **2**, 5−40 μm for **2-G**, and ca. 10 μm for **2-P** (Figures S12 and S23). Conducting the H_2 adsorption experiment at 77 K using sample **2-G** resulted in an adsorption isotherm very similar to the one observed for **2-P** (Figure 8a), which additionally confirms that in the case of the studied 2D MOF family, the crystal size has a significant impact on gas adsorption properties due to the kinetic effects corresponding to the number of pore entrances on the sides of the flake-shaped crystals.

CONCLUSIONS

In conclusion, we demonstrated that the diffusion-controlled preparation of 2D MOFs is a very efficient way for controlling their supramolecular structures using solvent-templating effect. Using this methodology we obtained the **Cu(hfipbb)** family of 2D MOFs which, depending on the solvent used, differed in stacking distance and stacking geometry of the layers. We investigated the gas adsorption properties of the developed 2D MOFs, which revealed relatively low N_2 and moderate CO_2 adsorption capacities. Remarkably, we observed a strong effect of crystal size on the N_2 adsorption capacity using a model 2D MOF system, which is most likely related to the limited number of pore entrances in the bigger flake-shaped crystals.

Moreover, we demonstrated the structural dynamics involving both in-plane and out-of-plane movement of 2D layers in the studied 2D MOF family triggered by the solvent exchange under mild conditions. Remarkably, the selectivity and yields of the investigated transformations depended on the type of introduced and replaced solvent molecules, which indicates the role of product stability as well as solvent permeability in controlling of these transformations. Further developments of this approach could lead to new procedures of

https://dx.doi.org/10.1021/acs.inorgchem.9b03472
Inorg. Chem. 2020, 59, 4389−4396

2D MOF postsynthetic modification by introduction of various functional molecules or assemblies capable of influencing the supramolecular stacking of the MOF layers.

Overall, we demonstrated a comprehensive case study of the family of Cu(II) carboxylate-based 2D MOFs involving the diffusion-based synthetic strategy, allowing for precise analysis of the role of solvent type, as an isolated variable, which might be a valuable tool for more in-depth understanding of MOFs formation in general.

■ ASSOCIATED CONTENT

Supporting Information

The Supporting Information is available free of charge at https://pubs.acs.org/doi/10.1021/acs.inorgchem.9b03472.

Crystal structure images (Figure S1), glass reactor image (Figure S2), IR spectra (Figures S3−S7), PXRD diffractograms (Figures S8−S11 and S13−S19), SEM image (Figure S12), gas adsorption isotherms (Figures S20−S22), and optical microscope images (Figure S23) (PDF)

Accession Codes

CCDC 1961201−1961205 contain the supplementary crystallographic data for this paper. These data can be obtained free of charge via www.ccdc.cam.ac.uk/data_request/cif, or by emailing data_request@ccdc.cam.ac.uk, or by contacting The Cambridge Crystallographic Data Centre, 12 Union Road, Cambridge CB2 1EZ, UK; fax: +44 1223 336033.

■ AUTHOR INFORMATION

Corresponding Author

Janusz Lewiński − *Institute of Physical Chemistry Polish Academy of Sciences, 01-224 Warsaw, Poland; Department of Chemistry Warsaw University of Technology, 00-664 Warsaw, Poland;* orcid.org/0000-0002-3407-0395; Email: lewin@ch.pw.edu.pl

Authors

Michał K. Leszczyński − *Institute of Physical Chemistry Polish Academy of Sciences, 01-224 Warsaw, Poland;* orcid.org/0000-0001-9339-101X

Iwona Justyniak − *Institute of Physical Chemistry Polish Academy of Sciences, 01-224 Warsaw, Poland*

Krzysztof Gontarczyk − *Department of Chemistry Warsaw University of Technology, 00-664 Warsaw, Poland*

Complete contact information is available at: https://pubs.acs.org/10.1021/acs.inorgchem.9b03472

Notes

The authors declare no competing financial interest.

■ ACKNOWLEDGMENTS

The authors would like to acknowledge the financial support from the Foundation for Polish Science Team Program cofinanced by the European Union under the European Regional Development Fund POIR.04.04.00-00-20C6/16-00. The authors would also like to thank A. Kornowicz for scientific discussion, W. Marynowski for assistance in SEM imaging, and V. Shejko for elemental analysis study.

■ REFERENCES

(1) Li, J.-R.; Kuppler, R. J.; Zhou, H.-C. Selective Gas Adsorption and Separation in Metal-Organic Frameworks. *Chem. Soc. Rev.* **2009**, *38*, 1477.

(2) Li, J.; Sculley, J.; Zhou, H. Metal-Organic Frameworks for Separations. *Chem. Rev.* **2012**, *112*, 869−932.

(3) Kreno, L. E.; Leong, K.; Farha, O. K.; Allendorf, M.; Van Duyne, R. P.; Hupp, J. T. Metal-Organic Framework Materials as Chemical Sensors. *Chem. Rev.* **2012**, *112*, 1105−1125.

(4) Morozan, A.; Jaouen, F. Metal Organic Frameworks for Electrochemical Applications. *Energy Environ. Sci.* **2012**, *5*, 9269−9290.

(5) Liu, J.; Chen, L.; Cui, H.; Zhang, J.; Zhang, L.; Su, C.-Y. Applications of Metal-Organic Frameworks in Heterogeneous Supramolecular Catalysis. *Chem. Soc. Rev.* **2014**, *43*, 6011−6061.

(6) Xia, W.; Mahmood, A.; Zou, R.; Xu, Q. Metal-Organic Frameworks and Their Derived Nanostructures for Electrochemical Energy Storage and Conversion. *Energy Environ. Sci.* **2015**, *8*, 1837−1866.

(7) Mukherjee, S.; Desai, A. V.; Ghosh, S. K. Potential of Metal-Organic Frameworks for Adsorptive Separation of Industrially and Environmentally Relevant Liquid Mixtures. *Coord. Chem. Rev.* **2018**, *367*, 82−126.

(8) Yang, C.; Kaipa, U.; Mather, Q. Z.; Wang, X.; Nesterov, V.; Venero, A. F.; Omary, M. A. Fluorous Metal-Organic Frameworks with Superior Adsorption and Hydrophobic Properties toward Oil Spill Cleanup and Hydrocarbon Storage. *J. Am. Chem. Soc.* **2011**, *133*, 18094−18097.

(9) Ding, M.; Cai, X.; Jiang, H.-L. Improving MOF Stability: Approaches and Applications. *Chem. Sci.* **2019**, *10*, 10209.

(10) Arhangelskis, M.; Katsenis, A. D.; Novendra, N.; Akimbekov, Z.; Gandrath, D.; Marrett, J. M.; Ayoub, G.; Morris, A. J.; Farha, O. K.; Friščić, T.; Navrotsky, A. Theoretical Prediction and Experimental Evaluation of Topological Landscape and Thermodynamic Stability of a Fluorinated Zeolitic Imidazolate Framework. *Chem. Mater.* **2019**, *31*, 3777−3783.

(11) Tchalala, M. R.; Bhatt, P. M.; Chappanda, K. N.; Tavares, S. R.; Adil, K.; Belmabkhout, Y.; Shkurenko, A.; Cadiau, A.; Heymans, N.; De Weireld, G.; Maurin, G.; Salama, K. N.; Eddaoudi, M. Fluorinated MOF Platform for Selective Removal and Sensing of SO_2 from Flue Gas and Air. *Nat. Commun.* **2019**, *10*, 1328.

(12) Noro, S.; Nakamura, T. Fluorine-Functionalized Metal-Organic Frameworks and Porous Coordination Polymers. *NPG Asia Mater.* **2017**, *9*, No. e433.

(13) Stock, N.; Biswas, S. Synthesis of Metal-Organic Frameworks (MOFs): Routes to Various MOF Topologies, Morphologies, and Composites. *Chem. Rev.* **2012**, *112*, 933−969.

(14) Karmakar, A.; Paul, A.; Pombeiro, A. J. L. Recent Advances on Supramolecular Isomerism in Metal Organic Frameworks. *CrystEngComm* **2017**, *19*, 4666−4695.

(15) Makal, T. A.; Yakovenko, A. A.; Zhou, H.-C. Isomerism in Metal-Organic Frameworks: "Framework Isomers". *J. Phys. Chem. Lett.* **2011**, *2*, 1682−1689.

(16) Bradshaw, D.; El-Hankari, S.; Lupica-Spagnolo, L. Supramolecular Templating of Hierarchically Porous Metal-Organic Frameworks. *Chem. Soc. Rev.* **2014**, *43*, 5431−5443.

(17) Kim, H.; Lah, M. S. Templated and Template-Free Fabrication Strategies for Zero-Dimensional Hollow MOF Superstructures. *Dalton Trans.* **2017**, *46*, 6146−6158.

(18) Hu, M.-L.; Masoomi, M. Y.; Morsali, A. Template Strategies with MOFs. *Coord. Chem. Rev.* **2019**, *387*, 415−435.

(19) Guo, X.; Geng, S.; Zhuo, M.; Chen, Y.; Zaworotko, M. J.; Cheng, P.; Zhang, Z. The Utility of the Template Effect in Metal-Organic Frameworks. *Coord. Chem. Rev.* **2019**, *391*, 44−68.

(20) Furukawa, H.; Cordova, K. E.; O'Keeffe, M.; Yaghi, O. M. The Chemistry and Applications of Metal-Organic Frameworks. *Science* **2013**, *341*, 1230444.

(21) Schneemann, A.; Bon, V.; Schwedler, I.; Senkovska, I.; Kaskel, S.; Fischer, R. A. Flexible Metal-Organic Frameworks. *Chem. Soc. Rev.* **2014**, *43*, 6062−6096.
(22) Nagarkar, S. S.; Desai, A. V.; Ghosh, S. K. Stimulus-Responsive Metal-Organic Frameworks. *Chem. - Asian J.* **2014**, *9*, 2358−2376.
(23) Coudert, F.-X. Responsive Metal-Organic Frameworks and Framework Materials: Under Pressure, Taking the Heat, in the Spotlight, with Friends. *Chem. Mater.* **2015**, *27*, 1905−1916.
(24) Zheng, W.; Tsang, C.; Lee, L. Y. S.; Wong, K. Two-Dimensional Metal-Organic Framework and Covalent-Organic Framework: Synthesis and Their Energy-Related Applications. *Mater. Today Chem.* **2019**, *12*, 34−60.
(25) Liu, W.; Yin, R.; Xu, X.; Zhang, L.; Shi, W.; Cao, X. Structural Engineering of Low-Dimensional Metal-Organic Frameworks: Synthesis, Properties, and Applications. *Adv. Sci.* **2019**, *6*, 1802373.
(26) Biradha, K.; Hongo, Y.; Fujita, M. Crystal-to-Crystal Sliding of 2D Coordination Layers Triggered by Guest Exchange. *Angew. Chem., Int. Ed.* **2002**, *41*, 3395−3398.
(27) Agarwal, R. A.; Mukherjee, S. Two-Dimensional Flexible Ni(II)-Based Porous Coordination Polymer Showing Single-Crystal to Single-Crystal Transformation, Selective Gas Adsorption and Catalytic Properties. *Polyhedron* **2016**, *105*, 228−237.
(28) Du, X.; Yan, B.; Wang, J.-Y.; Xi, X.; Wang, Z.; Zang, S.-Q. Layer-Sliding-Driven Crystal Size and Photoluminescence Change in a Novel SCC-MOF. *Chem. Commun.* **2018**, *54*, 5361−5364.
(29) Suh, M. P.; Moon, H. R.; Lee, E. Y.; Jang, S. Y. A Redox-Active Two-Dimensional Coordination Polymer: Preparation of Silver and Gold Nanoparticles and Crystal Dynamics on Guest Removal. *J. Am. Chem. Soc.* **2006**, *128*, 4710−4718.
(30) Leszczyński, M. K.; Kornowicz, A.; Prochowicz, D.; Justyniak, I.; Noworyta, K.; Lewiński, J. Straightforward Synthesis of Single-Crystalline and Redox-Active Cr(II)-Carboxylate MOFs. *Inorg. Chem.* **2018**, *57*, 4803−4806.
(31) Wang, S.-Q.; Yang, Q.-Y.; Mukherjee, S.; O'Nolan, D.; Patyk-Kaźmierczak, E.; Chen, K.-J.; Shivanna, M.; Murray, C.; Tang, C. C.; Zaworotko, M. J. Recyclable Switching between Nonporous and Porous Phases of a Square Lattice (Sql) Topology Coordination Network. *Chem. Commun.* **2018**, *54*, 7042−7045.
(32) Kondo, A.; Yashiro, T.; Okada, N.; Hiraide, S.; Ohkubo, T.; Tanaka, H.; Maeda, K. Selective Molecular-Gating Adsorption in a Novel Copper-Based Metal-Organic Framework. *J. Mater. Chem. A* **2018**, *6*, 5910−5918.
(33) Zhao, W.; Peng, J.; Wang, W.; Liu, S.; Zhao, Q.; Huang, W. Ultrathin Two-Dimensional Metal-Organic Framework Nanosheets for Functional Electronic Devices. *Coord. Chem. Rev.* **2018**, *377*, 44−63.
(34) Xu, M.; Yang, S.; Gu, Z. Two-Dimensional Metal-Organic Framework Nanosheets: A Rapidly Growing Class of Versatile Nanomaterials for Gas Separation, MALDI-TOF Matrix and Biomimetic Applications. *Chem. - Eur. J.* **2018**, *24*, 15131−15142.
(35) Zhao, M.; Huang, Y.; Peng, Y.; Huang, Z.; Ma, Q.; Zhang, H. Two-Dimensional Metal-Organic Framework Nanosheets: Synthesis and Applications. *Chem. Soc. Rev.* **2018**, *47*, 6267−6295.
(36) Xiao, P.; Xu, Y. Recent Progress in Two-Dimensional Polymers for Energy Storage and Conversion: Design, Synthesis, and Applications. *J. Mater. Chem. A* **2018**, *6*, 21676−21695.
(37) Köberl, M.; Cokoja, M.; Herrmann, W. A.; Kühn, F. E. From Molecules to Materials: Molecular Paddle-Wheel Synthons of Macromolecules, Cage Compounds and Metal-Organic Frameworks. *Dalton Trans.* **2011**, *40*, 6834−6859.
(38) Jiang, X.; Zhang, S.; Guo, J.-H.; Wang, X.-G.; Li, J.-S.; Du, M. Structural Diversity and Modulation of Metal-Organic Coordination Frameworks with a Flexible V-Shaped Dicarboxyl Building Block. *CrystEngComm* **2009**, *11*, 855−864.
(39) Pachfule, P.; Dey, C.; Panda, T.; Banerjee, R. Synthesis and Structural Comparisons of Five New Fluorinated Metal Organic Frameworks (F-MOFs). *CrystEngComm* **2010**, *12*, 1600−1609.
(40) Pachfule, P.; Das, R.; Poddar, P.; Banerjee, R. Solvothermal Synthesis, Structure, and Properties of Metal Organic Framework Isomers Derived from a Partially Fluorinated Link. *Cryst. Growth Des.* **2011**, *11*, 1215−1222.
(41) Ji, C.; Yin, L.; Huang, L.; Bai, X.; He, X.; Sheng, E. Syntheses, Structures and Properties of a New Cu(II) Coordination Polymer Based on 4,4′-(Hexafluoroisopropylidene)Bis(Benzoic Acid) Ligand. *J. Mol. Struct.* **2019**, *1183*, 292−297.
(42) Hayashi, T.; Hijikata, Y.; Page, A.; Jiang, D.; Irle, S. Theoretical Analysis of Structural Diversity of Covalent Organic Framework: Stacking Isomer Structures Thermodynamics and Kinetics. *Chem. Phys. Lett.* **2016**, *664*, 101−107.
(43) Prochowicz, D.; Nawrocki, J.; Terlecki, M.; Marynowski, W.; Lewiński, J. Facile Mechanosynthesis of the Archetypal Zn-Based Metal-Organic Frameworks. *Inorg. Chem.* **2018**, *57*, 13437−13442.
(44) Prochowicz, D.; Sokołowski, K.; Justyniak, I.; Kornowicz, A.; Fairen-Jimenez, D.; Friščić, T.; Lewiński, J. A Mechanochemical Strategy for IRMOF Assembly Based on Pre-Designed Oxo-Zinc Precursors. *Chem. Commun.* **2015**, *51*, 4032−4035.
(45) Sokołowski, K.; Bury, W.; Justyniak, I.; Fairen-Jimenez, D.; Sołtys, K.; Prochowicz, D.; Yang, S.; Schröder, M.; Lewiński, J. Permanent Porosity Derived from the Self-Assembly of Highly Luminescent Molecular Zinc Carbonate Nanoclusters. *Angew. Chem., Int. Ed.* **2013**, *52*, 13414−13418.
(46) Prochowicz, D.; Justyniak, I.; Kornowicz, A.; Kaczorowski, T.; Kaszkur, Z.; Lewiński, J. Construction of a Porous Homochiral Coordination Polymer with Two Types of Cu_nI_n Alternating Units Linked by Quinine: A Solvothermal and a Mechanochemical Approach. *Chem. - Eur. J.* **2012**, *18*, 7367−7371.
(47) Lewiński, J.; Kaczorowski, T.; Prochowicz, D.; Lipińska, T.; Justyniak, I.; Kaszkur, Z.; Lipkowski, J. Cinchona Alkaloid-Metal Complexes: Noncovalent Porous Materials with Unique Gas Separation Properties. *Angew. Chem., Int. Ed.* **2010**, *49*, 7035−7039.
(48) Kaczorowski, T.; Justyniak, I.; Lipińska, T.; Lipkowski, J.; Lewiński, J. Metal Complexes of Cinchonine as Chiral Building Blocks: A Strategy for the Construction of Nanotubular Architectures and Helical Coordination Polymers. *J. Am. Chem. Soc.* **2009**, *131*, 5393−5395.
(49) Agilent Technologies. *CrysAlisPro, Data Collection and Processing Software for Agilent X-ray Diffractometers*, ver. 1.171.35.21b; Agilent Technologies: 2012.
(50) Sheldrick, G. M. A Short History of SHELX. *Acta Crystallogr., Sect. A: Found. Crystallogr.* **2008**, *64*, 112−122.
(51) Sarkisov, L.; Harrison, A. Computational Structure Characterisation Tools in Application to Ordered and Disordered Porous Materials. *Mol. Simul.* **2011**, *37*, 1248−1257.
(52) Elsaidi, S. K.; Mohamed, M. H.; Banerjee, D.; Thallapally, P. K. Flexibility in Metal-Organic Frameworks: A Fundamental Understanding. *Coord. Chem. Rev.* **2018**, *358*, 125−152.

https://dx.doi.org/10.1021/acs.inorgchem.9b03472
Inorg. Chem. 2020, 59, 4389−4396